Full Spatial Characterization of Entangled Structured Photons

Xiaoqin Gao,[1,2] Yingwen Zhang,[1,3,*] Alessio D'Errico,[1] Alicia Sit,[1] Khabat Heshami,[3,1] and Ebrahim Karimi[1,3]
[1]Nexus for Quantum Technologies, University of Ottawa, K1N 5N6 Ottawa, Ontario, Canada
[2]Emerging Technologies Division, National Research Council of Canada, K1A 0R6, Ottawa, Ontario, Canada
[3]National Research Council of Canada, 100 Sussex Drive, K1A 0R6 Ottawa, Ontario, Canada

(Received 17 July 2023; accepted 9 January 2024; published 7 February 2024)

Vector modes are fully polarized modes of light with spatially varying polarization distributions, and they have found widespread use in numerous applications such as microscopy, metrology, optical trapping, nanophotonics, and communications. The entanglement of such modes has attracted significant interest, and it has been shown to have tremendous potential in expanding existing applications and enabling new ones. However, due to the complex spatially varying polarization structure of entangled vector modes (EVMs), a complete entanglement characterization of these modes remains challenging and time consuming. Here, we have used a time-tagging event camera to demonstrate the ability to completely characterize the entanglement of EVMs. Leveraging the camera's capacity to provide independent measurements for each pixel, we simultaneously characterize the entanglement of approximately 2.6×10^6 modes between a bipartite EVM through measuring only 16 observables in polarization. We reveal that EVMs can naturally generate various polarization-entangled Bell states. This achievement is an important milestone in high-dimensional entanglement characterization of structured light, and it could significantly impact the implementation of related quantum technologies. The potential applications of this technique are extensive, and it could pave the way for advancements in quantum communication, quantum imaging, and other areas where structured entangled photons play a crucial role.

DOI: 10.1103/PhysRevLett.132.063802

Quantum entanglement [1] is a remarkable feature of quantum theory that has become a cornerstone in photonic quantum information processing, encompassing quantum computation [2], quantum teleportation [3], quantum cryptography [4], and quantum dense coding [5]. Demonstrated across various degrees of freedom, including polarization [6], orbital angular momentum [7,8], path [9], and time-bin [10], photonic entanglement has gained prominence as technologies leveraging it become more integrated into daily life. Consequently, examining intricate entanglement structures and their applications is increasingly vital.

Distinct from homogeneously polarized light, vector modes (VMs) of light display a complex, spatially varying polarization structure [11]. Owing to their unique attributes, VMs have recently attracted attention in diverse fields such as nonlinear optics [12], high-resolution imaging [13], laser processing [14], classical or quantum communication [15–17], sharper focus spots [18,19], and quantum key distribution [20,21]. Two primary approaches to generate VMs include the intracavity method, which involves inserting mode-selection optical elements in a laser resonator [22–24], and the extracavity method, which entails transforming Gaussian modes into VMs using specialized optical elements like q plates [25,26] or a spatial light modulator combined with a Sagnac interferometer [27].

Entangled VMs (EVMs) have been demonstrated in [28,29], where polarization-entangled photon pairs are converted into VMs, transforming spatially homogeneous polarization entanglement into a complex, spatially variant polarization entanglement structure. However, thoroughly characterizing this spatially dependent entanglement without prior knowledge of the involved modes can be challenging, especially when the entanglement is in higher dimensional Hilbert spaces involving the superposition of multiple VMs. Utilizing the projective measurements approach [28], one will have to cycle through different q-plate combinations to determine the individual contributions of each mode. The number of measurements required will increase exponentially with an increase in the size of the involved Hilbert space. Alternatively, a full spatial scanning of the EVM can be performed where the polarization entanglement between every spatial point combination is characterized. Employing single-pixel detectors, such as avalanche photodiodes, necessitates $(N \times N)^2 \times 16$ measurements where $N \times N$ represents the number of spatial locations on each VM to be probed and 16 denotes the required polarization measurement combinations [30]. By using a triggerable intensified CCD (ICCD) camera, where a single-pixel detector triggers the ICCD, a total of $(N \times N) \times 16$ data acquisition runs will be required where in each run a polarization measurement is taken simultaneously between each pixel of the camera and the single-pixel detector. This is partially demonstrated in the case of a homogeneously polarized mode entangled to a VM [27,31].

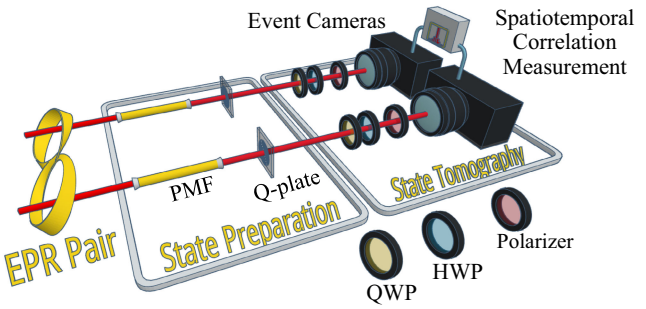

FIG. 1. Conceptual setup for the generation and characterization of vector mode entanglement. Einstein-Podolsky-Rosen (EPR) photon pairs entangled in the polarization degree of freedom are first spatially filtered by polarization-maintaining single-mode fibres (PMF) into the fundamental mode before being sent onto the q plates (with different topological charges) to create entangled structured photons. Polarization state tomography is performed using a combination of quarter-wave plates (QWP), half-wave plates (HWP), and polarizers with the photon pairs detected by time-tagging event cameras from which spatial-temporal information of the photons is collected. A spatial-temporal correlation measurement is then performed for each of the 16 combinations of polarization measurement. The density matrix and, subsequently, the Bell states for each pixel combination can then be determined.

Here, we present the full characterization of spatially dependent polarization entanglement between EVMs using only 16 data acquisition runs, where in each data acquisition run, a projection measurement on a polarization observable is made in parallel for each spatial location pair of the EVM. Facilitated by a time-tagging event camera, in each data acquisition run, a polarization measurement is taken simultaneously for all position combinations between the EVMs in a four-dimensional space. Covering approximately 40×40 pixels per VM, $\sim 2.6 \times 10^6$ modes between a bipartite entangled state are measured simultaneously. Various polarization-entangled Bell states have been generated naturally using the EVMs of this work. To showcase the versatility of our technique, we perform the characterization for various polarization topological patterns, including vector-vortex, lemon, star, and spiral polarization patterns, all exhibiting exceptional agreement with the anticipated entanglement pattern derived from theory. Compared to past demonstrations [27–29,31], this is the first time the four-dimensional spatially dependent polarization entanglement structure of EVMs is fully characterized without requiring prior knowledge of the involved VMs. The ability to perform this type of measurement within a reasonable time will have a profound impact on the fundamental studies of structured light entanglement as well as their potential applications in fields such as quantum communications and quantum sensing.

The conceptual diagram for the generation and characterization of spatially varying polarization-entangled photons is shown in Fig. 1. A polarization-entangled state with a Gaussian mode profile of the following form is first prepared,

$$|\Psi_0\rangle = \frac{1}{\sqrt{2}}(|H,V\rangle - |V,H\rangle) = \frac{i}{\sqrt{2}}(|L,R\rangle - |R,L\rangle), \quad (1)$$

where $|L,R\rangle = |L\rangle_s \otimes |R\rangle_i$ with $|L\rangle$ and $|R\rangle$ denoting left- and right-circular polarization, and the subscripts s and i denoting the signal and idler photons, respectively. This initial polarization-entangled state can be chosen to be any of the four Bell states; we have chosen to use this particular antisymmetric state simply because this is the output state of our photon source (see the Supplemental Material [32] for more details). The setup of Fig. 1 does not need to be changed for different initial Bell states, and the theoretical calculations to follow can also be easily modified based on the initial state.

The unitary action of a q plate with topological charge q acting on a circularly polarized Gaussian mode can be written as [35]

$$\hat{U}_q^\delta \cdot \begin{bmatrix} |L\rangle \\ |R\rangle \end{bmatrix} = F_0(r)\cos\left(\frac{\delta}{2}\right)\begin{bmatrix} |L\rangle \\ |R\rangle \end{bmatrix} + i\sin\left(\frac{\delta}{2}\right)F_q(r) \times \begin{bmatrix} e^{-i2q\theta}|R\rangle \\ e^{i2q\theta}|L\rangle \end{bmatrix}, \quad (2)$$

where $F_0(r)$ and $F_q(r)$ determine the radial profiles of the unconverted and converted modes, respectively—here, we considered q plates wherein the local optical axis distribution of the liquid crystals is $\alpha(\theta) = q\theta$. Both $F_0(r)$ and $F_q(r)$ can be expressed analytically in terms of hypergeometric Gauss modes [36]. However, for q plates with low q values, within a good approximation, both radial functions can be expressed in terms of the Laguerre-Gauss modes possessing azimuthal indices of 0 and $2q$, and radial index zero at $z = 0$, respectively, i.e., $F_q(r)e^{\pm i2q\theta} \equiv \mathrm{LG}_{0,\pm 2q}(r,\theta)$ [35]. $\delta \in [0,\pi]$ is the optical retardation of the q plate, which can be tuned based on the voltage applied to the q plates [37]. Therefore, sending each photon onto different q plates yields the following complex space-varying polarization-entangled state,

$$|\Psi_f\rangle = \frac{1}{\sqrt{2}}\left(\hat{U}_{q_s}^{\delta_s}\cdot|L\rangle_s\hat{U}_{q_i}^{\delta_i}\cdot|R\rangle_i - \hat{U}_{q_s}^{\delta_s}\cdot|R\rangle_s\hat{U}_{q_i}^{\delta_i}\cdot|L\rangle_i\right). \quad (3)$$

Here, $\hat{U}_{q_s}^{\delta_s}$ and $\hat{U}_{q_i}^{\delta_i}$ denote the signal and idler q-plate actions, respectively—note that the global U(1) phase of $\pi/2$ is omitted. The four parameters of $\{q_s, \delta_s, q_i, \delta_i\}$ determine the polarization entanglement state between signal and idler photons. For instance, setting $q_s = q_i = 1/2$ and $\delta_s = \delta_i = \pi/2$, the polarization Einstein-Podolsky-Rosen (EPR) state is transformed into the radial and azimuthal entangled state, i.e., $(|\text{radial, azimuthal}\rangle - |\text{azimuthal, radial}\rangle)/\sqrt{2}$.

To characterize the spatially varying entanglement between the entangled photons, polarization state tomography is performed using 16 different combinations of polarization measurement. Each photon is then collected

by a time-tagging event camera (TPX3CAM [38,39]) placed in the near field of the two q plates from which spatial-temporal information about the photons is recorded. A spatial-temporal correlation measurement is then performed between the two cameras for each of the 16 polarization measurements from which the spatially varying density matrix and, subsequently, the Bell states contributions can be determined.

In this Letter, we demonstrate the entanglement characterization for two q-plate settings: the case of when both q plates are perfectly tuned ($\delta_s = \delta_i = \pi$) and when both are partially tuned ($\delta_s = \delta_i = \pi/2$). For two tuned q plates with topological charges q_s and q_i applied to the signal and idler photons, respectively, Eq. (3) can be rewritten as a superposition of the four Bell states, $|\phi^{\pm}\rangle = (1/\sqrt{2})(|H\rangle_s|H\rangle_i \pm |V\rangle_s|V\rangle_i)$ and $|\psi^{\pm}\rangle = (1/\sqrt{2})(|H\rangle_s|V\rangle_i \pm |V\rangle_s|H\rangle_i)$, as

$$|\Psi_f\rangle = F_{q_s,q_i}(r_s, r_i)[\sin 2(q_s\theta_s - q_i\theta_i)|\phi^+\rangle - \cos 2(q_s\theta_s - q_i\theta_i)|\psi^-\rangle], \tag{4}$$

where $F_{q_s,q_i}(r_s, r_i) = F_{q_s}(r_s)F_{q_i}(r_i)$, and (r_s, θ_s) and (r_i, θ_i) are the transverse coordinates of signal and idler photons.

For the partially tuned case, ($\delta_s = \delta_i = \pi/2$), we can rewrite Eq. (3) as

$$\begin{aligned}|\Psi_f\rangle = \frac{1}{2}\Big\{ & -F_{q_s,q_i}(r_s,r_i)\sin 2(q_s\theta_s - q_i\theta_i)|\phi^+\rangle \\ & + [F_{0,0}(r_s,r_i) - F_{q_s,q_i}(r_s,r_i)\sin 2(q_s\theta_s - q_i\theta_i)]|\psi^-\rangle \\ & + [F_{0,q_i}(r_s,r_i)\sin 2q_i\theta_i - F_{q_s,0}(r_s,r_i)\sin 2q_s\theta_s]|\phi^-\rangle \\ & + [F_{0,q_i}(r_s,r_i)\cos 2q_i\theta_i - F_{q_s,0}(r_s,r_i)\cos 2q_s\theta_s]|\psi^+\rangle\Big\}.\end{aligned} \tag{5}$$

Detailed calculations can be found in the Supplemental Material [32].

The Bell state contributions for EVMs generated with tuned q plates depend only on the azimuthal degree of freedom (d.o.f.), θ_s and θ_i, and of course, the plates, topological charges q_s, q_i, while both ϕ^- and ψ^+ states make no contributions. For partially tuned q plates, the situation is more complex since all four Bell states make contributions. Indeed, Bell states are a function of both the azimuthal d.o.f., θ_s and θ_i, and the radial d.o.f., r_s and r_i.

In the experimental demonstration (see Supplemental Material [32] for the detailed experimental setup), a single time-tagging camera was employed as an alternative to the originally proposed dual-camera setup. Each photon of the EVM pair was directed toward a corner of the camera, encompassing an area of roughly 40×40 pixels. An initial temporal correlation measurement was conducted to identify photon pairs using the position and time data of each photon captured by the camera. This was followed by a spatial correlation measurement conducted in cylindrical polar coordinates, which will give a better visualization of the predicted patterns as given by Eqs. (4) and (5). This procedure was repeated for 16 distinct polarization measurement combinations, as required for biphoton polarization state tomography [30]. The quantum state tomography for EVMs generated with q plates of topological charges $q_s = 1/2$ and $q_i = 1$ is illustrated in Fig. 2. The measured spatial correlation between signal and idler photons in the azimuthal d.o.f. θ, with radial d.o.f. r summed over, is presented for the 16 different polarization combinations employed in polarization state tomography; see Fig. 2(a). Correlations in the radial d.o.f. exhibited minimal variation between distinct polarization measurements and are, therefore, not depicted here, but can be found in the Supplemental Material [32]. Subsequently, an azimuthal angle-dependent density matrix was reconstructed using a maximum likelihood method (as detailed in Sec. VI of [30]), and to simplify visualization, the corresponding Bell state decomposition is displayed in Fig. 2(c). We observe azimuthally that the measured Bell state contributions oscillate between the $|\psi^-\rangle$ and $|\phi^+\rangle$ states, with negligible contributions from the $|\phi^-\rangle$ and $|\psi^+\rangle$ states. This outcome aligns well with the theoretical expression reported in Eq. (4). A concurrence is also measured for every θ_s and θ_i combination of the EVM with an average value of 0.540 ± 0.005. Compared to the ideal value of 1, this reduced concurrence is likely a result of experimental imperfections, such as imperfections in the q plate, which may introduce a radial dependence of the entangled state, as well as a nonuniform retardation. Imperfect alignment, the slightly nonuniform quantum efficiency across the pixels of the camera, and the quality of the initial Bell state used in generating the EVM will all have an effect on the measured concurrence. Results for two partially tuned q plates with topological charges $q_s = 1/2$ and $q_i = 1$ are displayed in Figs. 2(d)–2(f). Because of the increased complexity of the spatially variant structure and sensitivity to optical alignment, the state tomography results are noisier, yet they still demonstrate reasonable agreement with theoretical expectations. The average concurrence of the EVM is measured to be 0.517 ± 0.005.

Figure 3 displays the experimentally measured Bell state decomposition for EVMs generated using both tuned and partially tuned q plates at various combinations of topological charges. The probability amplitudes of the Bell states are mapped onto a torus for a more compact and clearer depiction of the cyclic nature of the azimuthal angle of polar coordinates (θ_s, θ_i). For the measured spatial correlations of all q-plate combinations, please refer to the Supplemental Material [32].

From our results, we can see that it is possible to determine the involved charges of unknown q plates based on the patterns seen in the measured probability plot for the

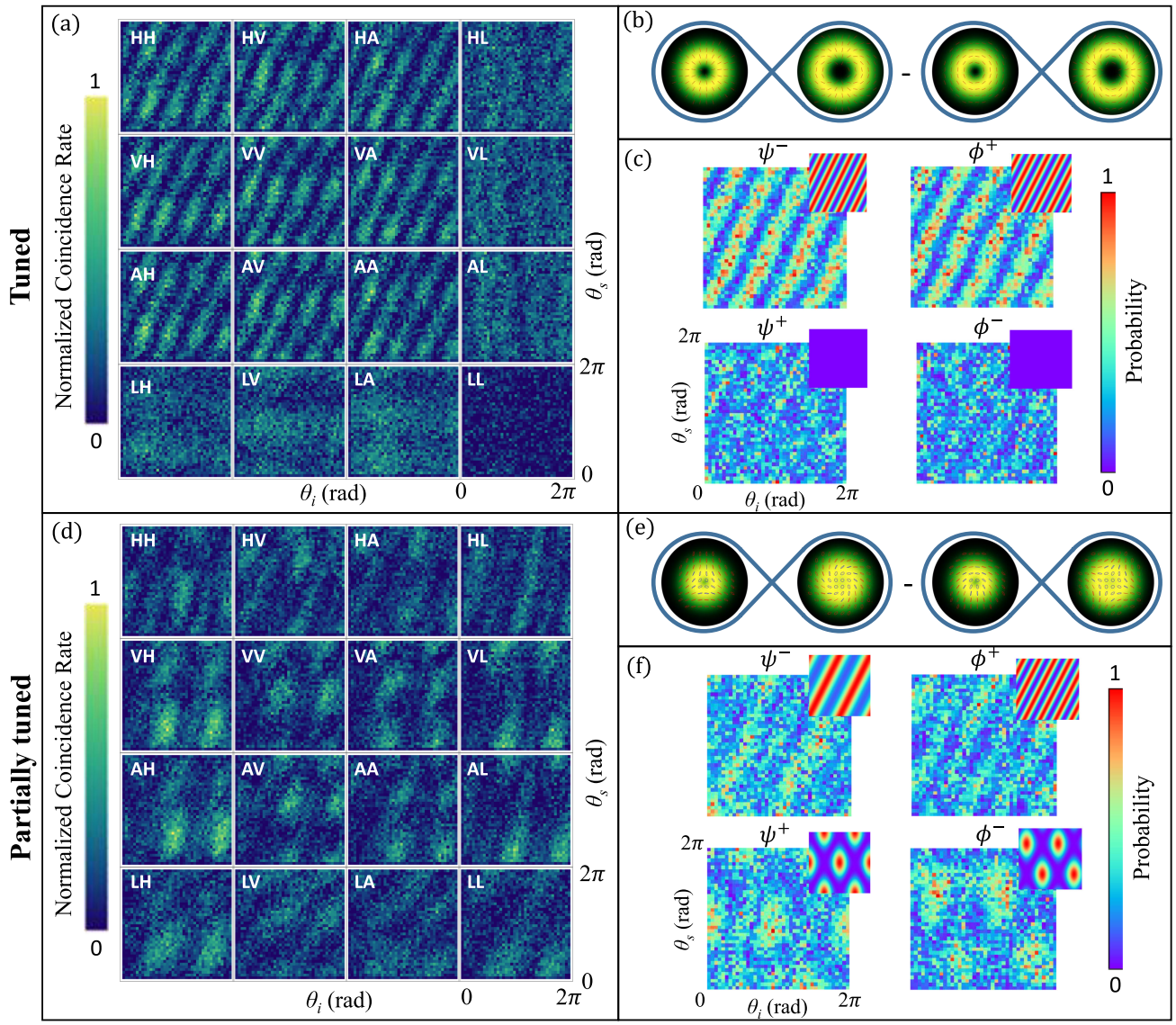

FIG. 2. Measured spatial correlations and entanglement characterization for biphoton with spatially varying polarization states generated via two q plates. (a) Two-photon spatial correlations between two entangled vector modes measured in the azimuthal degree of freedom from 16 different polarization measurements. Two tuned q plates ($\delta_s = \delta_i = \pi$) with topological charges $q_i = 1$ and $q_s = 1/2$ are used to generate the entangled vector-vortex photons. (b) Graphical representation of the polarization patterns overlaid on the photon probability distribution for an input EPR pair in the antisymmetric Bell state. (c) Reconstructed probabilities for the four Bell states $\{|\psi^+\rangle, |\psi^-\rangle, |\phi^+\rangle, |\phi^-\rangle\}$. The insets are the respective theoretical probabilities. (d)–(f) Corresponding results for two partially tuned q plates ($\delta_s = \delta_i = \pi/2$) with topological charges $q_i = 1$ and $q_s = 1/2$. Red lines in (b) and red (blue) ellipses in (e) show the major axes of the polarization.

four Bell states. For tuned q plates with a single charge, the involved charges can be determined by looking at the frequency and orientation of the bright stripes in the ψ^- and ϕ^+ basis. In cases where the q plate contains a superposition of charges, a brute-force approach may be necessary. The tomography patterns of different charge combinations can be calculated theoretically. Then, using the theoretically generated patterns, a comparison can be drawn between theory and experiment to identify the best matching case. The process may be sped up if one can identify distinct structures in the tomography results based on the charges involved. For instance, in our case of partially tuned q plates, a superposition of charges 0 and q, patterns seen in the tomography results, such as the frequency and orientation of the stripes and spots, can provide clues to the charges involved. Ultimately, the challenge of finding the contributing modes experimentally now shifts to a theoretical and computational problem, which can be performed significantly faster. This, however, is beyond the scope of this work and will require further investigation.

One significant limitation of the current demonstration is the low efficiency of single-photon detection, i.e., the

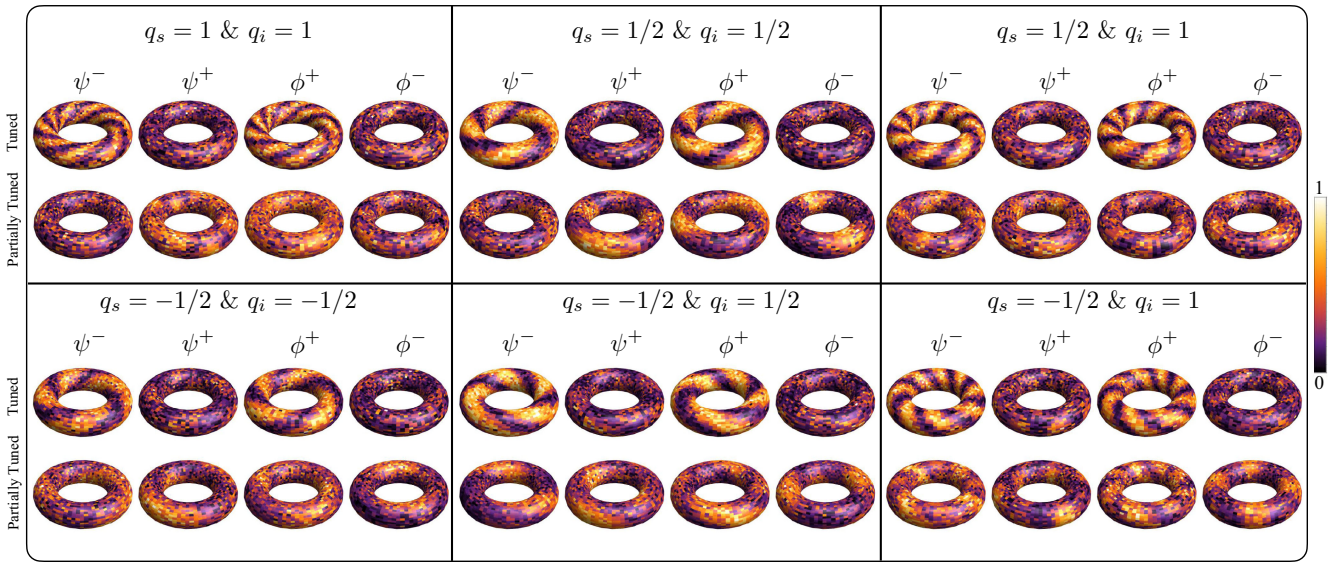

FIG. 3. The experimental results for the probabilities of the four Bell states. The Bell state probabilities at different azimuthal angles between the two entangled vector modes are mapped onto a torus. The vector modes are generated for a combination of q plates with a fractional topological charge of $q = -1/2$, $1/2$, or 1 in each path.

camera, which results in significant noise and extended data acquisition times of 8 min per data acquisition run. The camera's low efficiency of approximately 8% [34], combined with the need to couple polarization-entangled photons into single-mode fibers with a coupling efficiency of around 30%, only provides a coincidence efficiency of 0.06%. To improve the system's performance, a potential first step would be to generate entangled photons directly from fibers through spontaneous four-wave mixing [40], eliminating the losses associated with fiber coupling. This modification could result in an order of magnitude improvement in coincidence efficiency and, consequently, a reduction in data acquisition time. Moreover, with the coincidence efficiency scaling quadratically relative to the single-photon efficiency, further improvements could be achievable with the development of more sensitive cameras in the near future, allowing for entanglement characterization to be performed in mere seconds.

In conclusion, we have successfully demonstrated the generation and characterization of the nonuni form transverse polarization entanglement between various classes of VMs in a scan-free manner. This is the first experiment in which the four-dimensional entanglement structure of EVMs is fully characterized and has revealed previously unseen entanglement structures. Past experiments could only perform the characterization in either two or three dimensions [27–29,31]. The demonstrated method can be invaluable for quickly characterizing spatially varying entanglement in EVMs, which are gaining interest in various high-dimensional quantum systems such as quantum communication and quantum imaging. We utilized spatial-temporal correlation measurements on data collected by a time-tagging event camera to perform polarization state tomography on approximately 2.6×10^6 (40×40) spatial modes using only 16 data acquisition runs. In our work, it has been observed that various polarization-entangled Bell states can naturally arise from EVMs. The measurement results agreed well with theoretical predictions. Future improvements to the detection efficiency of time-tagging camera technology could potentially enable real-time state tomography on EVMs by splitting the photons onto multiple cameras, with each camera measuring a different polarization. These developments would significantly enhance the capabilities of quantum communication and quantum imaging systems. The local entanglement measurements in our system could be exploited to enhance the sensitivity of photonic gears [41,42]. Our study also shows some promising applications—for example, quantum sensing of birefringent materials, and the generation of high-dimensional topological structures such as 4D skyrmions.

This work was supported by the Canada Research Chairs (CRC), the High Throughput and Secure Networks (HTSN) Challenge Program at the National Research Council of Canada, and the Joint Centre for Extreme Photonics (JCEP). The authors would like to thank Ryan Hogan for helping with coding during the data analysis, and Paul Corkum, Felix Hufnagel, Dilip Paneru, and Frédéric Bouchard for their valuable discussions. K. H. acknowledges that the National Research Council of Canada (NRC) headquarters is located on the traditional unceded territory of the Algonquin Anishinaabe and Mohawk people.

*Corresponding author: yzhang6@uottawa.ca

[1] A. Einstein, B. Podolsky, and N. Rosen, Can quantum-mechanical description of physical reality be considered complete?, Phys. Rev. **47**, 777 (1935).

[2] Robert Raussendorf and Hans J. Briegel, A one-way quantum computer, Phys. Rev. Lett. **86**, 5188 (2001).

[3] Charles H. Bennett, Gilles Brassard, Claude Crépeau, Richard Jozsa, Asher Peres, and William K. Wootters, Teleporting an unknown quantum state via dual classical and Einstein-Podolsky-Rosen channels, Phys. Rev. Lett. **70**, 1895 (1993).

[4] Artur K. Ekert, Quantum cryptography based on Bell's theorem, Phys. Rev. Lett. **67**, 661 (1991).

[5] Charles H. Bennett and Stephen J. Wiesner, Communication via one- and two-particle operators on Einstein-Podolsky-Rosen states, Phys. Rev. Lett. **69**, 2881 (1992).

[6] Paul G. Kwiat, Aephraim M. Steinberg, and Raymond Y. Chiao, Observation of a "quantum eraser": A revival of coherence in a two-photon interference experiment, Phys. Rev. A **45**, 7729 (1992).

[7] Ebrahim Karimi, Daniel Giovannini, Eliot Bolduc, Nicolas Bent, Filippo M. Miatto, Miles J. Padgett, and Robert W. Boyd, Exploring the quantum nature of the radial degree of freedom of a photon via Hong-Ou-Mandel interference, Phys. Rev. A **89**, 013829 (2014).

[8] Yingwen Zhang, Filippus S Roux, Thomas Konrad, Megan Agnew, Jonathan Leach, and Andrew Forbes, Engineering two-photon high-dimensional states through quantum interference, Sci. Adv. **2**, e1501165 (2016).

[9] T. B. Pittman, D. V. Strekalov, A. Migdall, M. H. Rubin, A. V. Sergienko, and Y. H. Shih, Can two-photon interference be considered the interference of two photons?, Phys. Rev. Lett. **77**, 1917 (1996).

[10] J. Brendel, N. Gisin, W. Tittel, and H. Zbinden, Pulsed energy-time entangled twin-photon source for quantum communication, Phys. Rev. Lett. **82**, 2594 (1999).

[11] Qiwen Zhan, Cylindrical vector beams: From mathematical concepts to applications, Adv. Opt. Photonics **1**, 1 (2009).

[12] A. Bouhelier, M. Beversluis, A. Hartschuh, and L. Novotny, Near-field second-harmonic generation induced by local field enhancement, Phys. Rev. Lett. **90**, 013903 (2003).

[13] Weibin Chen and Qiwen Zhan, Numerical study of an apertureless near field scanning optical microscope probe under radial polarization illumination, Opt. Express **15**, 4106 (2007).

[14] Yuichi Kozawa and Shunichi Sato, Optical trapping of micrometer-sized dielectric particles by cylindrical vector beams, Opt. Express **18**, 10828 (2010).

[15] Vincenzo D'ambrosio, Eleonora Nagali, Stephen P Walborn, Leandro Aolita, Sergei Slussarenko, Lorenzo Marrucci, and Fabio Sciarrino, Complete experimental toolbox for alignment-free quantum communication, Nat. Commun. **3**, 961 (2012).

[16] Osvaldo Jiménez Farías, Vincenzo D'Ambrosio, Caterina Taballione, Fabrizio Bisesto, Sergei Slussarenko, Leandro Aolita, Lorenzo Marrucci, Stephen P Walborn, and Fabio Sciarrino, Resilience of hybrid optical angular momentum qubits to turbulence, Sci. Rep. **5**, 8424 (2015).

[17] Bienvenu Ndagano, Isaac Nape, Mitchell A Cox, Carmelo Rosales-Guzman, and Andrew Forbes, Creation and detection of vector vortex modes for classical and quantum communication, J. Lightwave Technol. **36**, 292 (2018).

[18] R. Dorn, S. Quabis, and G. Leuchs, Sharper focus for a radially polarized light beam, Phys. Rev. Lett. **91**, 233901 (2003).

[19] Haifeng Wang, Luping Shi, Boris Lukyanchuk, Colin Sheppard, and Chong Tow Chong, Creation of a needle of longitudinally polarized light in vacuum using binary optics, Nat. Photonics **2**, 501 (2008).

[20] C. E. R. Souza, C. V. S. Borges, A. Z. Khoury, J. A. O. Huguenin, L. Aolita, and S. P. Walborn, Quantum key distribution without a shared reference frame, Phys. Rev. A **77**, 032345 (2008).

[21] Giuseppe Vallone, Vincenzo D'Ambrosio, Anna Sponselli, Sergei Slussarenko, Lorenzo Marrucci, Fabio Sciarrino, and Paolo Villoresi, Free-space quantum key distribution by rotation-invariant twisted photons, Phys. Rev. Lett. **113**, 060503 (2014).

[22] Kyosuke Sakai and S. Noda, Optical trapping of metal particles in doughnut-shaped beam emitted by photonic-crystal laser, Electron. Lett. **43**, 107 (2007), https://digital-library.theiet.org/content/journals/10.1049/el_20073012.

[23] Eiji Miyai, Kyosuke Sakai, Takayuki Okano, Wataru Kunishi, Dai Ohnishi, and Susumu Noda, Lasers producing tailored beams, Nature (London) **441**, 946 (2006).

[24] Seita Iwahashi, Yoshitaka Kurosaka, Kyosuke Sakai, Kyoko Kitamura, Naoki Takayama, and Susumu Noda, Higher-order vector beams produced by photonic-crystal lasers, Opt. Express **19**, 11963 (2011).

[25] Filippo Cardano, Ebrahim Karimi, Sergei Slussarenko, Lorenzo Marrucci, Corrado de Lisio, and Enrico Santamato, Polarization pattern of vector vortex beams generated by q-plates with different topological charges, Appl. Opt. **51**, C1 (2012).

[26] Filippo Cardano, Ebrahim Karimi, Lorenzo Marrucci, Corrado de Lisio, and Enrico Santamato, Generation and dynamics of optical beams with polarization singularities, Opt. Express **21**, 8815 (2013).

[27] Robert Fickler, Mario Krenn, Radek Lapkiewicz, Sven Ramelow, and Anton Zeilinger, Real-time imaging of quantum entanglement, Sci. Rep. **3**, 1914 (2013).

[28] Vincenzo D'Ambrosio, Gonzalo Carvacho, Francesco Graffitti, Chiara Vitelli, Bruno Piccirillo, Lorenzo Marrucci, and Fabio Sciarrino, Entangled vector vortex beams, Phys. Rev. A **94**, 030304 (2016).

[29] Francesco Graffitti, Vincenzo D'Ambrosio, Massimiliano Proietti, Joseph Ho, Bruno Piccirillo, Corrado de Lisio, Lorenzo Marrucci, and Alessandro Fedrizzi, Hyperentanglement in structured quantum light, Phys. Rev. Res. **2**, 043350 (2020).

[30] J. B. Altepeter, E. R. Jeffrey, and P. G. Kwiat, Photonic state tomography, edited by P. R. Berman and C. C. Lin, *Advances in Atomic, Molecular, and Optical Physics* Vol. 52 (Academic Press, London, 2005), pp. 105–159.

[31] Robert Fickler, Radek Lapkiewicz, Sven Ramelow, and Anton Zeilinger, Quantum entanglement of complex photon polarization patterns in vector beams, Phys. Rev. A **89**, 060301 (2014).

[32] See Supplemental Material at http://link.aps.org/supplemental/10.1103/PhysRevLett.132.063802 for more

theoretical and experimental detail, which includes Refs. [33,34].

[33] Ali Anwar, Chithrabhanu Perumangatt, Fabian Steinlechner, Thomas Jennewein, and Alexander Ling, Entangled photon-pair sources based on three-wave mixing in bulk crystals, Rev. Sci. Instrum. **92**, 041101 (2021).

[34] Victor Vidyapin, Yingwen Zhang, Duncan England, and Benjamin Sussman, Characterisation of a single photon event camera for quantum imaging, Sci. Rep. **13**, 1009 (2023).

[35] Ebrahim Karimi, Bruno Piccirillo, Lorenzo Marrucci, and Enrico Santamato, Light propagation in a birefringent plate with topological charge, Opt. Lett. **34**, 1225 (2009).

[36] Ebrahim Karimi, Gianluigi Zito, Bruno Piccirillo, Lorenzo Marrucci, and Enrico Santamato, Hypergeometric-Gaussian modes, Opt. Lett. **32**, 3053 (2007).

[37] Sergei Slussarenko, Anatoli Murauski, Tao Du, Vladimir Chigrinov, Lorenzo Marrucci, and Enrico Santamato, Tunable liquid crystal q-plates with arbitrary topological charge, Opt. Express **19**, 4085 (2011).

[38] https://www.amscins.com/tpx3cam/.

[39] Andrei Nomerotski, Imaging and time stamping of photons with nanosecond resolution in timepix based optical cameras, Nucl. Instrum. Methods Phys. Res., Sect. A **937**, 26 (2019).

[40] Hiroki Takesue and Kyo Inoue, Generation of polarization-entangled photon pairs and violation of Bell's inequality using spontaneous four-wave mixing in a fiber loop, Phys. Rev. A **70**, 031802 (2004).

[41] Vincenzo D'ambrosio, Nicolo Spagnolo, Lorenzo Del Re, Sergei Slussarenko, Ying Li, Leong Chuan Kwek, Lorenzo Marrucci, Stephen P Walborn, Leandro Aolita, and Fabio Sciarrino, Photonic polarization gears for ultra-sensitive angular measurements, Nat. Commun. **4**, 2432 (2013).

[42] Raouf Barboza, Amin Babazadeh, Lorenzo Marrucci, Filippo Cardano, Corrado de Lisio, and Vincenzo D'Ambrosio, Ultra-sensitive measurement of transverse displacements with linear photonic gears, Nat. Commun. **13**, 1080 (2022).